ACS NANO
Cite This: ACS Nano 2019, 13, 9016–9027
www.acsnano.org

ARTICLE

A Robust Aqueous Core–Shell–Shell Coconut-like Nanostructure for Stimuli-Responsive Delivery of Hydrophilic Cargo

Chen Tan,[†] Mohammad Arshadi,[†] Michelle C. Lee,[†] Mary Godec,[†] Morteza Azizi,[†] Bing Yan,[†] Hamed Eskandarloo,[†] Ted W. Deisenroth,[‡] Rupa Hiremath Darji,[‡] Toan Van Pho,[‡] and Alireza Abbaspourrad*[,†]

[†]Department of Food Science, Cornell University, Stocking Hall, Ithaca, New York 14853, United States
[‡]BASF Corporation, 500 White Plains Road, Tarrytown, New York 10591, United States

Supporting Information

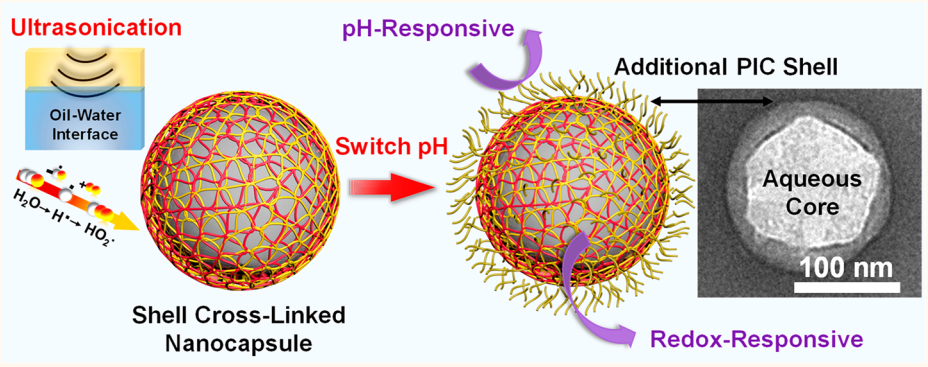

ABSTRACT: **Conventional delivery systems for hydrophilic material still face critical challenges toward practical applications, including poor retention abilities, lack of stimulus responsiveness, and low bioavailability. Here, we propose a robust encapsulation strategy for hydrophilic cargo to produce a wide class of aqueous core–shell–shell coconut-like nanostructures featuring excellent stability and multifunctionality. The numerous active groups (−SH, $-NH_2$, and −COOH) of the protein–polysaccharide wall material enable the formation of shell-cross-linked nanocapsules enclosing a liquid water droplet during acoustic cavitation. A subsequent pH switch can trigger the generation of an additional shell through the direct deposition of non-cross-linked protein back onto the cross-linked surface. Using anthocyanin as a model hydrophilic bioactive, these nanocapsules show high encapsulation efficiency, loading content, tolerance to environmental stresses, biocompatibility, and high cellular uptake. Moreover, the composite double shells driven by both covalent bonding and electrostatics provide the nanocapsules with pH/redox dual stimuli-responsive behavior. Our approach is also feasible for any shell material that can be cross-linked *via* ultrasonication, offering the potential to encapsulate diverse hydrophilic functional components, including bioactive molecules, nanocomplexes, and water-dispersible inorganic nanomaterials. Further development of this strategy should hold promise for designing versatile nanoengineered core–shell–shell nanoplatforms for various applications, such as the oral absorption of hydrophilic drugs/nutraceuticals and the smart delivery of therapeutics.**

KEYWORDS: *core–shell–shell, nanostructure, hydrophilic material, cross-linking, interfacial complexation, stimuli-responsive*

Although hydrophilic bioactive agents, such as drugs, nutraceuticals, natural colorants, peptides, enzymes, proteins, water-dispersible biopolymer complexes, and inorganic nanomaterials can bring about health benefits, their use is often limited by the susceptibility to chemical or biochemical degradation under certain environmental conditions (*e.g.*, pH, ionic strength, temperature, and oxygen) or within the gastrointestinal tract, low bioavailability, short biological half-lives in the circulatory system, and inadequate tissue distribution.[1−5] Encapsulation in colloidal systems can be an efficient approach for the protection and controlled delivery of bioactive agents. However, in contrast with the significant advances made in the development of delivery systems for hydrophobic bioactives, there have been far fewer

Received: April 19, 2019
Accepted: July 25, 2019
Published: July 25, 2019

DOI: 10.1021/acsnano.9b03049
ACS Nano 2019, 13, 9016–9027

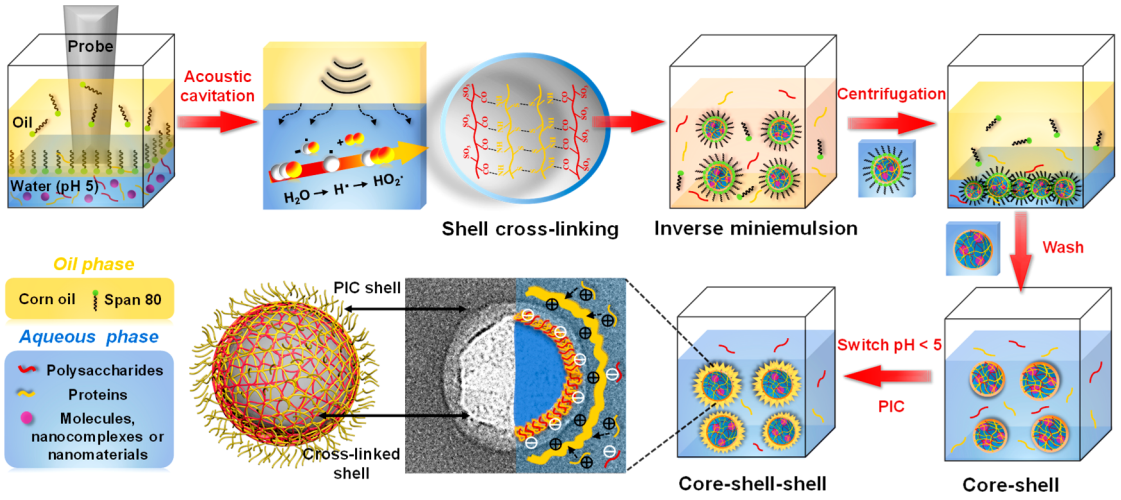

Figure 1. General strategy for the synthesis of an aqueous core−shell−shell nanostructured platform *via* sequential cross-linking and PIC. Here, the combination of polysaccharides and proteins is taken as an example to fabricate a cross-linked nanocapsule shell, followed by the direct deposition of excess non-cross-linked proteins to form an additional PIC shell layer.

effective systems for hydrophilic materials due to the strong tendency of hydrophilic compounds to leak out into the external aqueous phase and the difficulty in producing such systems at an industrial scale.[6,7]

To date, several major strategies have been explored to encapsulate hydrophilic compounds. One involves traditional multiple emulsions (particularly water-in-oil-in-water emulsions) in which the hydrophilic compounds are trapped within the internal dispersed water droplets.[8] Unfortunately, such multiple emulsions are thermodynamically unstable, causing the water droplets to be susceptible to flocculation, coalescence, and Ostwald ripening. Additionally, this system requires a substantial amount of encapsulation material, and the final product is thus low loading in bioactives. Solid lipid nanoparticles are also limited by the low loading capacity of hydrophilic compounds, and the requirement of high temperature during preparation to melt the lipid.[9] Another strategy consists of complex structured polymeric particles,[10] hollow "layer-by-layer" capsules,[11,12] or hydrogels[13,14] generated by either directly mixing or using a sacrificial template (*e.g.*, polystyrene, $CaCO_3$, SiO_2). However, since the complexes are primarily fabricated from weak electrostatic attractions, these structures can easily dissociate or degrade when the environmental pH and ionic strength change. On the other hand, the removal of the template typically occurs under harsh conditions (*e.g.*, the strong basicity of $CaCO_3$), which could impair the stability of the loaded bioactives.

Other major strategies include mini-emulsion interfacial polymerization, which is an emerging technique that allows the direct encapsulation of liquid water droplets containing hydrophilic agents within polymer shells.[15−17] With the aid of microfluidic techniques, it is also possible to fabricate polymeric capsules with controlled size and morphology.[18−20] However, because of the size limitation of microfluidic channels, it is extremely difficult to obtain capsules in the nanometer range, which are the ideal size for drug delivery.[21,22] Furthermore, most interfacial polymerization requires the careful choice of specific pairs of polymerizing monomers and block copolymers to produce polymerized capsules, which largely restricts this strategy from being generally adopted for a wide range of shell materials and particularly biopolymers. Exposure of the core contents to the monomers and organic solvents can also make the active molecules lose bioactivity. Thus, there is still a pressing need to develop an effective strategy and multifunctional nanosystems for hydrophilic bioactive delivery.

To tackle this need, we explore a general, powerful, and green encapsulation strategy to engineer a robust nanocarrier for hydrophilic bioactive agents that does not require the multistep emulsification, substantial dilution, template core removal, the use of microfluidic devices, organic solvents, or monomers/synthetic copolymers. Instead, our approach involves the ultrasonication-initiated cross-linking of materials dispersed at an oil−water interface followed by polyelectrolytic interfacial complexation (PIC), as illustrated in Figure 1. Taking the combination of natural polysaccharides and proteins as an example, we first prepare a two-phase system of an oil phase and an aqueous phase composed of biopolymers. The pH of the individual polysaccharide and protein solutions is adjusted to 5 in order to make these molecules negatively charged, preventing the formation of polyelectrolyte complexes *via* electrostatic interaction after mixing. During acoustic cavitation, the abundant active groups (*e.g.*, −SH, $-NH_2$, and −COOH) in these biopolymers allow them to form a cross-linked nanocapsule shell enclosing a liquid water droplet in an inverse mini-emulsion. The isolated water compartments (aqueous core) allow for loading of hydrophilic cargo, while the dense cross-linked shell contributes to the high cargo retention efficiency by inhibiting leakage of the entrapped cargos during oil removal. Subsequently, we modulate the ionization of the dispersed shell materials by lowing the pH of the aqueous nanocapsule suspension, causing any non-cross-linked biopolymers (protein in this case) that remain in solution to directly deposit back onto the cross-linked shell *via* interfacial complexation, creating an additional PIC shell.

In this manner, we are able to achieve a distinct class of nanoscale aqueous core−shell−shell coconut-like structures, which features both excellent stability and multifunctionality. Importantly, our strategy can provide a general route to fabricate a variety of core−shell−shell nanostructures from different shell materials, as long as they can be cross-linked by ultrasonication. We also demonstrate the versatility of this nanostructure as an efficient delivery nanoplatform for a wide

DOI: 10.1021/acsnano.9b03049
ACS Nano 2019, 13, 9016−9027

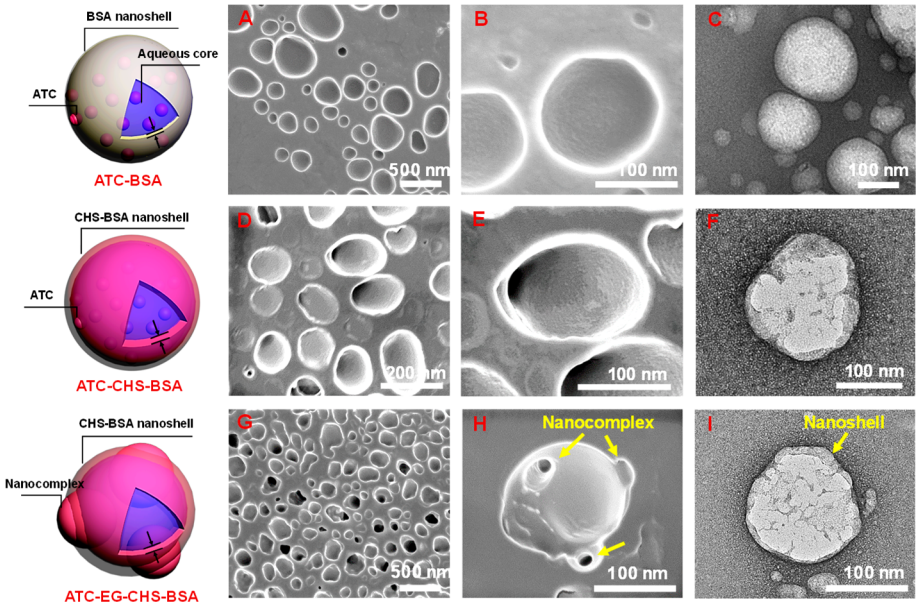

Figure 2. Morphology of core−shell nanocapsules featuring the incorporation of ATC and nanocomplexes. Schematic illustrating the shell cross-linked structures and corresponding morphology of (A−C) ATC-BSA, (D−F) ATC-CHS-BSA, and (G−I) ATC-EG-CHS-BSA observed by SEM (A, B, D, E, G, H) and TEM (C, F, I) images.

Table 1. Average Particle Size, ζ Potential, Polydispersity Index, Encapsulation Efficiency, Capsule Yield, Retention Efficiency, and ATC Recovery of Various Formulations

	particle size (nm)	ζ potential (mV)	polydispersity index	yield (%)	encapsulation efficiency (%)	retention efficiency (%)	recovery (%)
ATC-BSA	185.7 ± 1.6	−10.2 ± 0.2	0.32 ± 0.01	21.7 ± 1.8	33.5 ± 2.3	42.1 ± 1.5	96.7 ± 2.5
ATC-CHS-BSA	149.4 ± 1.2	−60.4 ± 1.3	0.20 ± 0.01	34.7 ± 1.5	47.4 ± 1.6	68.4 ± 1.8	97.4 ± 1.1
ATC-EG-CHS-BSA	147.0 ± 0.4	−55.5 ± 1.1	0.18 ± 0.01	38.2 ± 1.3	54.6 ± 1.4	73.3 ± 2.1	96.8 ± 1.7

array of hydrophilic bioactive molecules, nanocomplexes, and water-dispersible inorganic particles.

RESULTS AND DISCUSSION

Shell Cross-Linked Nanocapsule with an Aqueous Core. Our synthesis began with the preparation of shell cross-linked nanocapsule with an aqueous core. Sonochemistry is a valuable technique for the synthesis of core−shell micro/nanocapsules because ultrasound can both emulsify immiscible liquids and produce a cavitation effect that can generate reactive free radicals (*e.g.*, OH•, H•, and HO_2•) to cross-link the dispersed materials at the air−water or oil−water interface.[23−25] However, conventional sonochemical synthesis has been significantly limited by some constraints with respect to the use of materials (usually only proteins) and a low degree of cross-linking despite many attempts to optimize the experimental conditions.[26,27] Regarding these issues, we aimed to reinforce the protein cross-linked shell by introducing polysaccharides, which feature hydroxyl and carboxyl functional groups that could provide additional intermolecular interactions with the proteins *via* amide linkage and hydrogen bonding, in addition to the interprotein disulfide cross-linking reaction. Another major challenge is that the sonochemical approach has traditionally been specialized for the encapsulation of hydrophobic compounds.[26−28] Prior to this study, we were unsure whether our proposed polysaccharide/protein cross-linked shell would be sufficiently strong to retain the hydrophilic compounds in the aqueous core.

For proof-of-concept, we used bovine serum albumin (BSA) and chondroitin sulfate (CHS) as shell materials, as they contain a large number of active groups, including −SH and $-NH_2$ in the protein and −COOH and −OH in the polysaccharide. As a model hydrophilic molecule, anthocyanin (ATC) was chosen due to its potential as both a pharmacological agent and natural food colorant, though it demonstrates extremely poor stability under harsh conditions.[29,30] To evaluate the potential of our encapsulation strategy for nanocomplexes, we also prepared co-pigmentation nanocomplexes (50−90 nm) by complexing ATC with the co-pigment ethyl gallate (EG) and CHS (Figures S1 and S2, see Supporting Information for more details). The CHS-BSA nanocapsules loaded with either ATC or nanocomplexes are denoted as ATC-CHS-BSA and ATC-EG-CHS-BSA, respectively. For comparison, we also prepared ATC-loaded BSA nanocapsules (ATC-BSA) whose shell was cross-linked by BSA alone without the reinforcement of a polysaccharide. The structural schematic of these formulations is shown in Figure 2.

Scanning electron microscopy (SEM) images in Figure 2 show that the ATC-BSA and ATC-CHS-BSA capsules exhibited defined spherical structures and smooth surfaces. In the presence of nanocomplexes, the capsules (ATC-EG-CHS-BSA) still maintained well-dispersed and nanoscale dimensions (90−150 nm). Higher magnification demonstrated the successful incorporation of nanocomplexes into these nanocapsules, which appeared to bulge due to the encapsulated contents (Figure 2H). Transmission electron microscopy (TEM) images further confirmed the formation of the core−

DOI: 10.1021/acsnano.9b03049
ACS Nano 2019, 13, 9016−9027

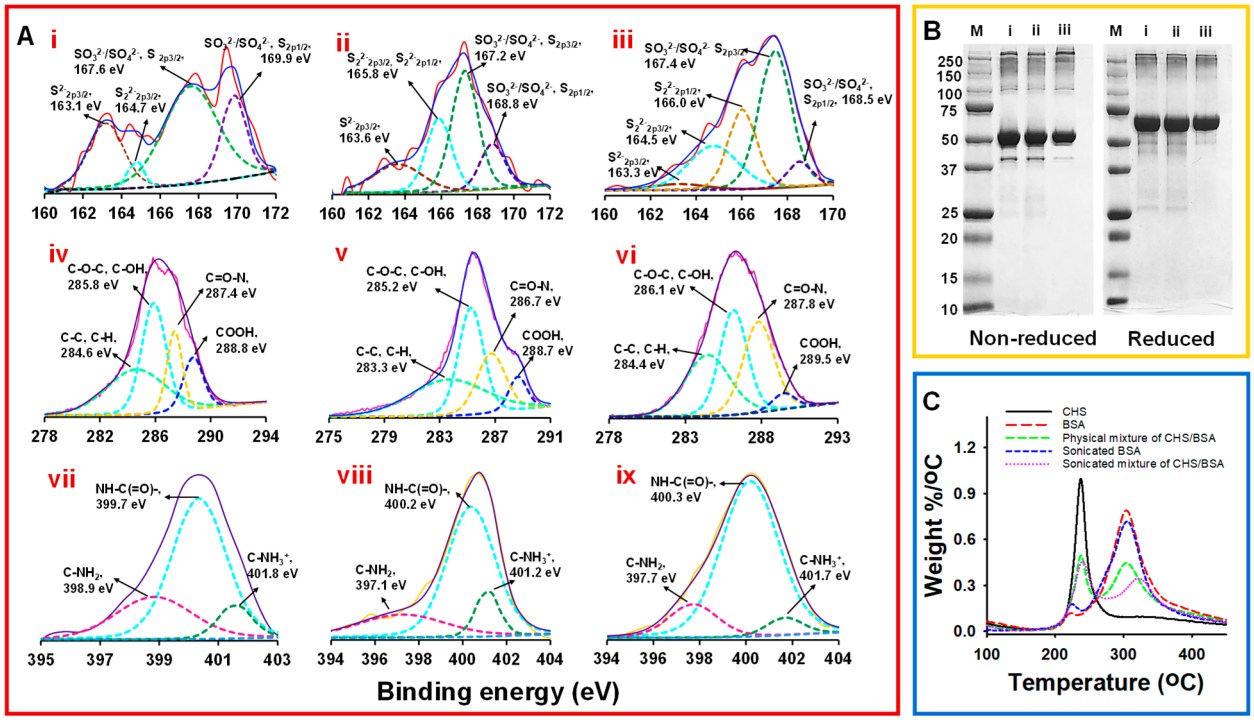

Figure 3. Characterization of CHS-BSA cross-linking. (A) High-resolution XPS spectra of the (i, ii, vii) physical mixture of CHS-BSA, (ii, v, viii) sonicated BSA, and (iii, vi, ix) sonicated CHS-BSA: (i–iii) S 2p, (iv–vi) C 1s, and (vii–ix) N 1s. (B) The SDS-PAGE electrophoretic profile of (line (i)) native BSA, (line (ii)) sonicated BSA, and (line (iii)) sonicated CHS-BSA under nonreduced and reduced conditions with *β*-mercaptoethanol. Molecular masses of the marker (M) are indicated in kDa. (C) First derivative thermogravimetric curves.

shell nanostructure with a thin cross-linked nanoshell (6–13 nm) surrounding the inner aqueous core. Good dispersity (polydispersity index < 0.2) and high negative charge (*ζ* potential < −50 mV) were also observed for ATC-CHS-BSA and ATC-EG-CHS-BSA from dynamic light scattering analysis (Table 1).

By introducing additional interactions between the CHS and protein, the capsule yield of ATC-CHS-BSA and ATC-EG-CHS-BSA considerably increased by 59.9% and 76.0% compared to ATC-BSA (Table 1), respectively. At the same time, the reinforced cross-linked shell of CHS-BSA can effectively maintain ATC in the aqueous core during preparation and long-term storage (1 month), with much higher encapsulation and retention efficiency than those by the BSA shell alone (Table 1). On the other hand, we should point out that the reactive free radicals generated during acoustic cavitation could not only cross-link the biopolymers but also degrade the loaded small bioactives. We therefore measured the residual ATC in the formulations after preparation and found that few ATC was lost (recovery >95%) by the ultrasonic treatment. This indicated that the ultrasonic condition we used (8 min at 300 W cm^{-2}) did not impair the stability of the loaded bioactive.

We believe that the formation of a reinforced cross-linked shell is the key criterion enabling the high encapsulation of hydrophilic bioactives in the aqueous core. To verify how much the cross-linking is improved by the polysaccharide in comparison with BSA alone, we employed various techniques to characterize the molecular interactions between the CHS and BSA. Figure 3A presents the X-ray photoelectron spectroscopy (XPS) spectra of physical mixture of CHS-BSA, sonicated BSA, and sonicated mixture of CHS-BSA. The S 2p spectra (Figure 3 A, i–iii) showed that the intensity of the peak (~166 eV) related to the −S−S− bond of cysteine residues increased in both sonicated BSA and CHS-BSA compared to their physical mixture, while the intensity of the −SH group (~163.3 eV) decreased, suggesting that ultrasonication induced the conversion of −SH to −S−S−.[31,32] For the −COOH group, after ultrasonication its intensity in CHS-BSA at the binding energy of 289.5 eV became weaker (Figure 3A, iv–vi). At the same time, we can see an increase in the intensity of the amide bond (O═C−N) in CHS-BSA at ~400.3 eV as well as the decreased intensity of the amine group (C-NH_2) at ~397.7 eV (Figure 3A, vii–ix). This observation suggested the formation of amide bonding between $-NH_2$ and −COOH by ultrasonication.[33,34] Based on the area integral peak of C-NH_2 (~397 eV), the cross-linking degrees of sonicated BSA and CHS-BSA were calculated to be around 8.4% and 14.2%, respectively.

Electrophoretic profiles obtained by SDS-PAGE (Figure 3B, left panel) show a clear reduction in the mobility and intensity of two bands from 37 to 50 kDa in the sonicated BSA-CHS mixture (line iii) as compared to the native BSA (line i) and sonicated BSA alone (line ii). This indicated the cross-linking reaction between the two materials under ultrasonication, leading to high molecular weight moieties. After reduction with *β*-mercaptoethanol (Figure 3B, right panel), high molecular weight proteins at 100 kDa disappeared, demonstrating the existence of intermolecular disulfide bonds. However, no fragmentation was detected in the region below 50 kDa for the sonicated BSA-CHS mixture, while a smear appeared for native BSA and sonicated BSA, implying nonreducible cross-linking between CHS and BSA. The thermogravimetric analysis (Figure 3C) also showed that the peak in BSA at around 304 °C shifted toward higher temperature (~322 °C) after sonicating with CHS. All these characteristics confirmed the

DOI: 10.1021/acsnano.9b03049
ACS Nano 2019, 13, 9016–9027

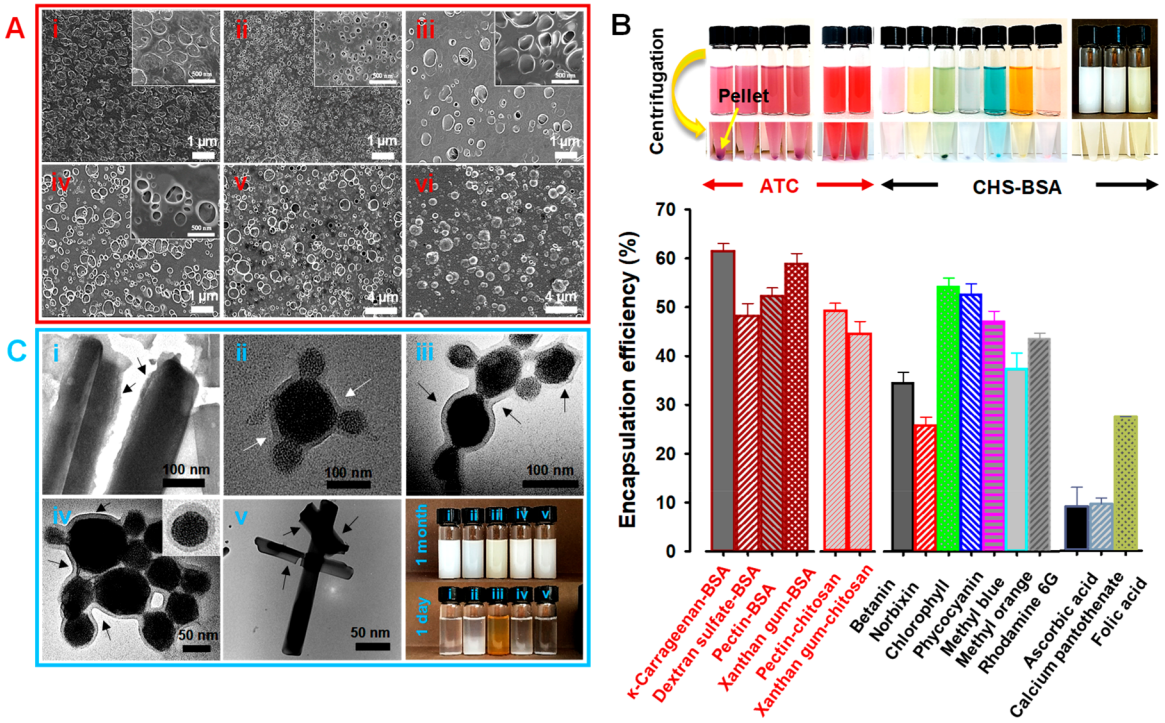

Figure 4. A variety of core−shell nanostructures. (A) SEM images of various capsules formed with (i) κ-carrageenan-BSA, (ii) dextran sulfate-BSA, (iii) pectin-BSA, (iv) xanthan gum-BSA, (v) pectin-chitosan, and (vi) xanthan gum-chitosan. (B) Encapsulation efficiency of ATC in capsules formed with different shell materials as well as the encapsulation of other hydrophilic compounds in CHS-BSA capsules. The inset shows the visual appearance of the corresponding formulations and capsule pellets collected at the bottom of centrifugal tubes after centrifugation at 15,000 *g* for 10 min. (C) TEM images of various nanostructures incorporating: (i) halloysite nanotubes, (ii) CuO nanoparticles, (iii) Fe_3O_4 nanoparticles, (iv) TiO_2 nanoparticles (inset: a single encapsulated nanoparticle), and (v) TiO_2 nanotubes. The inset on the bottom right shows the comparison of inorganic nanomaterials before and after loading in the CHS-BSA nanoshells for 1 day and 1 month of storage, respectively. In this figure, all the cross-linked nanoshells composed of polysaccharide-BSA were formed at pH 5 (except the folic acid loading at pH 8), while the fully polysaccharide cross-linked shells were formed at pH 2. Data represent mean ± SD, *n* = 3.

existence of strong cross-linking between BSA and CHS through interprotein disulfide bonding and amide linkage, which promoted the encapsulation capacity of the cross-linked shell for hydrophilic bioactives.

Universality of This Strategy. Since the cross-linking reaction can be initiated among various functional groups by ultrasonication, our strategy should work for other shell materials as well. To demonstrate the versatility of this approach, we introduced other polysaccharides to cross-link BSA, including κ-carrageenan, dextran sulfate, pectin, and xanthan gum. SEM imaging shows that these polysaccharides can successfully generate a variety of cross-linked capsules after ultrasonication with BSA (Figure 4A, i−iv). The capsule size and ATC encapsulation efficiency greatly depend on the type of polysaccharide (Figure 4B and Figures S3 and S4). The cross-linked reaction can also occur solely between polysaccharides such as the combinations of pectin-chitosan and xanthan gum-chitosan (Figure 4A, v−vi), which allowed the formation of a dense polysaccharide shell for high encapsulation of ATC (Figure 4B).

Next, we demonstrated that our strategy can be applied to encapsulate other hydrophilic compounds including betanin, norbixin, chlorophyll, phycocyanin, ascorbic acid, calcium pantothenate, folic acid, methyl blue, methyl orange, and rhodamine 6G (their molecular structure shown in Figure S5). The resulting CHS-BSA nanocapsule suspensions were clear (Figure 4B, inset), suggesting the potential application for transparent food and pharmaceutical products. Note, all of these compounds could demonstrate non-interaction or even electrostatic repulsion against the CHS and BSA of the nanocapsules because they are either neutral or negatively charged at the formulated pH (Figure S6). Despite that, the nanocapsules still had good encapsulation (10−60%) even for the smallest bioactives with molecular weights within 100−900 Da (Figure S5). This indicated that the resulting polysaccharide/protein cross-linked shell has a dense network (*i.e.*, low permeability), enabling strong physical entanglements to these hydrophilic compounds.

We also evaluated the possibility of incorporating water-dispersible inorganic nanomaterials into the CHS-BSA cross-linked shell. Here, we synthesized a few typical inorganic nanomaterials, including halloysite nanotubes, Fe_3O_4 nanoparticles, CuO nanoparticles, TiO_2 nanoparticles, and TiO_2 nanotubes, which were modified with different ligands (see detailed experimental procedures in the Supporting Information). Different from the severe aggregation and stack of bare nanomaterials (Figure S7), the encapsulated ones dispersed well. Furthermore, we found that all of them can be successfully incorporated in a 5−10 nm shell (Figure 4C). Generally, the surface of inorganic nanomaterials must be modified using ligands to avoid the loss of functionality brought about by poor water dispersibility or serious aggregation,[35−37] but the types of ligands are quite diverse depending on the nanomaterial composition. In this case, our

DOI: 10.1021/acsnano.9b03049
ACS Nano 2019, 13, 9016−9027

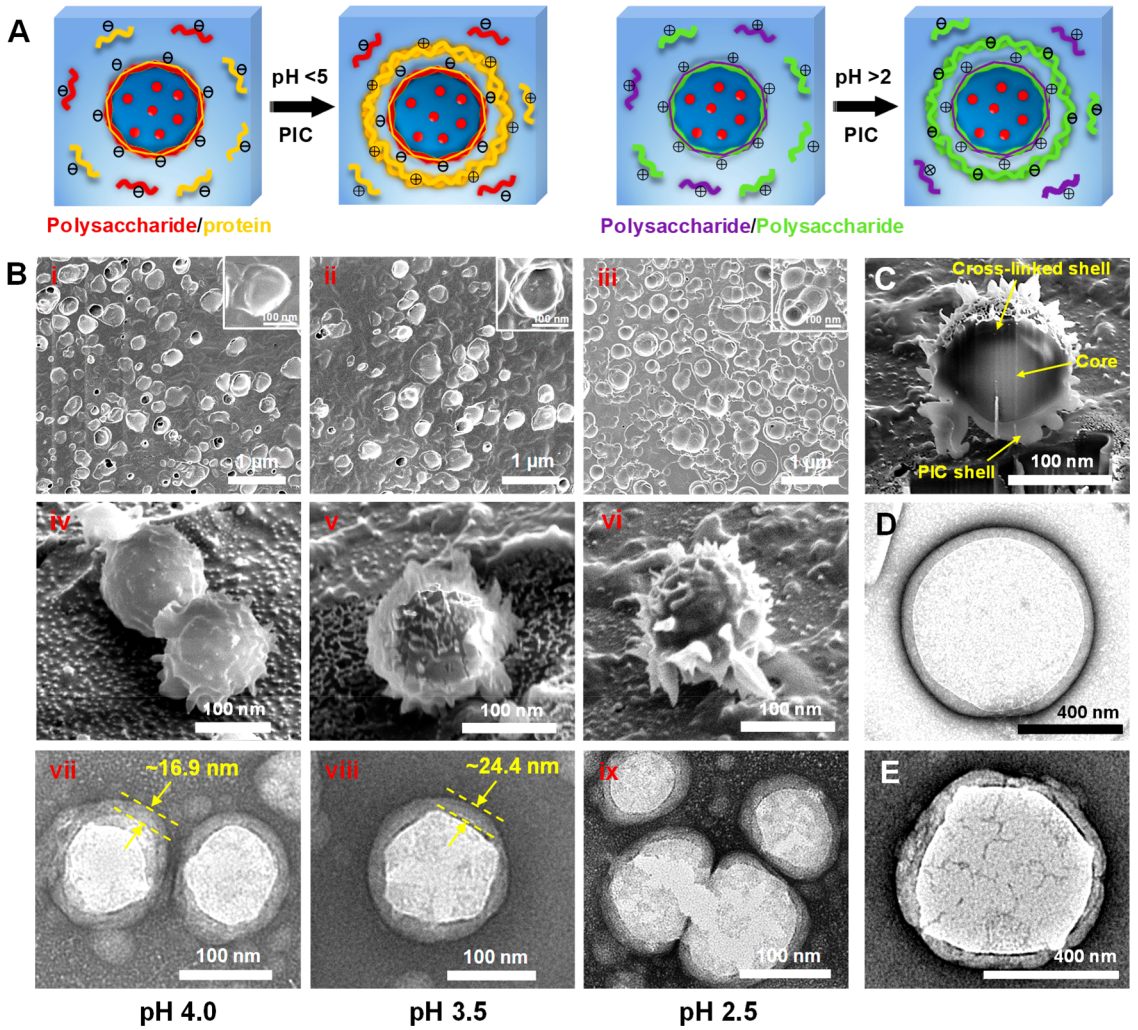

Figure 5. An additional PIC shell generated on the surface of the shell cross-linked nanocapsules. (A) Schematic illustrating the electrostatic deposition of non-cross-linked polyelectrolytes back onto the surface of the cross-linked shell after the pH was switched. The combinations of polysaccharide/protein and polysaccharide/polysaccharide were taken as an example. (B) Morphological evolution of the nanocapsules with decreasing pH from 5.0 to (i, iv, vii) 4.0, (ii, v, viii) 3.5, and (iii, vi, ix) 2.5. (i–iii) SEM, (iv–vi) cryo-SEM, and (vii-ix) TEM images, respectively. (C) A cross-sectional image produced by cryo-FIB milling, showing high magnification of the core–shell–shell nanostructure. Here, the capsules were made by decreasing the pH from 5.0 to 2.5, with CHS and BSA as the shell materials, that is, ATC-CHS-BSA. (D, E) TEM images of fully polysaccharide capsules made of (D) pectin-chitosan and (E) xanthan gum-chitosan formed by increasing the pH from 2.0 to 4.6.

method proved to be universal for encapsulating various inorganic nanomaterials regardless of their type or ligands as well as significantly simplifying the surface functionalization process of the nanomaterials. More importantly, after incorporation into the cross-linked shell, these nanomaterials remained stable for up to 1 month in contrast to the quick precipitation of non-encapsulated ones within 1 day (Figure 4C and Figure S8). The encapsulated nanomaterials also possess great colloidal stability under physiological condition (0.3 M NaCl, 10 mM phosphate buffer, and pH 7.4) (Figure S9). Another main application of the incorporation into the cross-linked shell is to impart additional functionalities to the nanomaterials, such as significantly improved UV ray blocking of the TiO_2 nanoparticles and nanotubes for the use of these composites in sunscreen (Figures S10 and S11).

Interfacial Complexation on Cross-Linked Shell. We note that although the degree of ultrasonication-induced cross-linking was enhanced by our strategy, more than 60% of the initially added BSA and CHS remains in solution. Taking a cue from the difference in acid ionization constant of the various shell materials, we were inspired to create an additional PIC shell layer by simply switching the pH of the as-prepared shell cross-linked nanocapsule suspension. For instance, the isoelectric points of BSA and pK_a of CHS are approximately 4.5 and 2.6, respectively. If we adjust the pH of the capsule suspension (*e.g.*, ATC-CHS-BSA) from 5.0 to lower values (2.5–4.5), the non-cross-linked BSA molecules that remain in solution would become positively charged due to the ionization of the NH_2 groups, which then interfacially complex with the existing negatively charged nanocapsules (Figure 5A). This hypothesis was verified by the progressive decrease in the negative charge of the nanocapsules and their size increase with decreasing pH (Figure S12). SEM imaging further shows that when the pH was adjusted to lower than 5, the majority of the nanocapsules had an additional shell layer of BSA (Figure 5B, i–iii). At low pH, the cryo-SEM images reveal the rougher surface of the nanocapsules due to the adsorption of BSA molecules (Figure 5B, iv–vi). From our cross-sectional

DOI: 10.1021/acsnano.9b03049
ACS Nano 2019, 13, 9016–9027

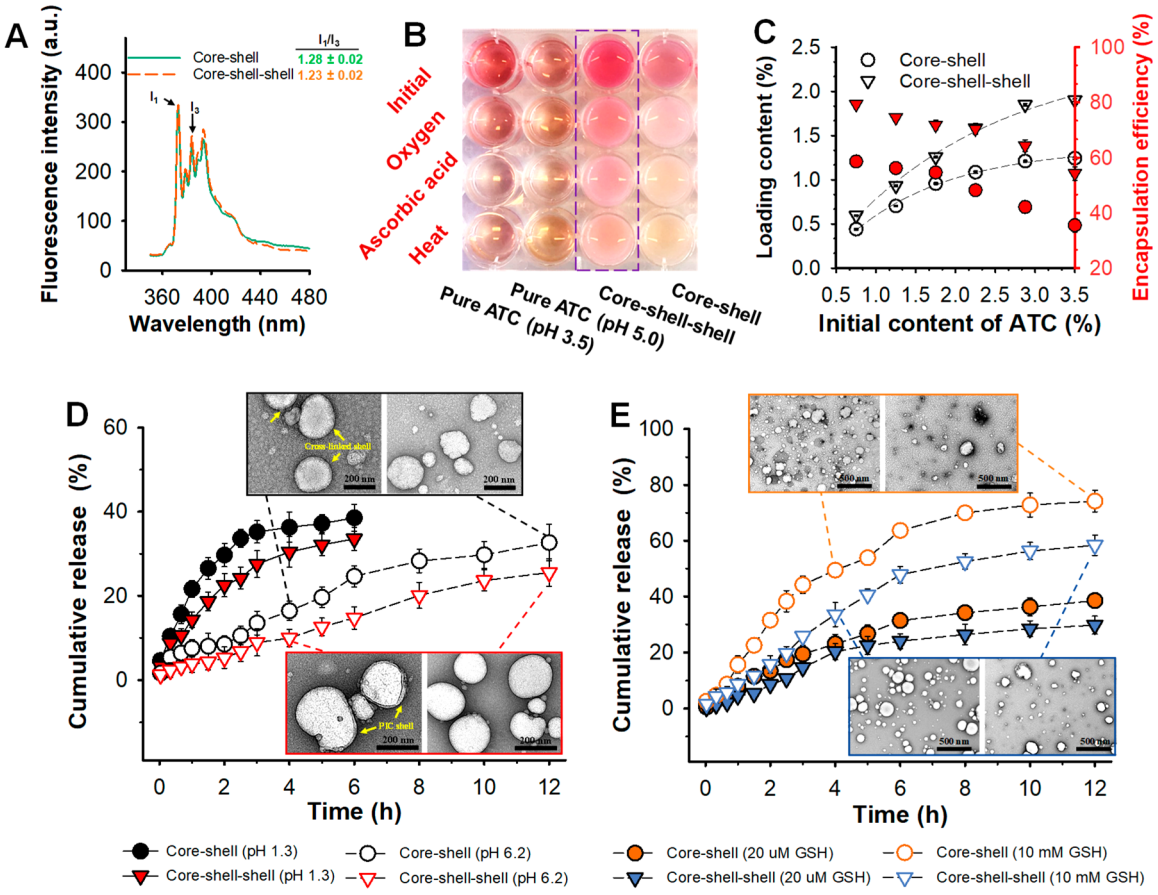

Figure 6. Performance comparison of core−shell and core−shell−shell nanocapsules. (A) Fluorescence spectra of pyrene and the polarity parameter I_1/I_3 of various nanocapsule suspensions. (B) Environmental responsiveness of the nanocapsules: auto-oxidation at room temperature for 1 week with exposure to oxygen; incubation at 40 °C for 2 d in the presence of ascorbic acid, and heat at 80 °C for 6 h. (C) Loading content and encapsulation efficiency as a function of the initial ATC content. (D) The pH-responsive release of ATC from the nanocapsules at pH 1.3 and 6.2. (E) The reduction-responsive release of ATC from the nanocapsules in the presence of GSH at 20 μM and 10 mM at pH 6.2. Insets in (D, E) are the TEM images showing the structural change of the nanocapsules after 4 and 12 h incubation. In this figure, the core−shell and core−shell−shell nanocapsules refer to the ATC-CHS-BSA formulation prepared at pH 5.0 and 3.5, respectively. Data represent mean ± SD, n = 3.

observation of the nanocapsules using cryo-focused ion beam (FIB) milling, we can clearly visualize a core−shell−shell coconut-like nanostructure (Figure 5C). TEM images also demonstrate the added PIC shell deposited on the capsules, with a thickness of that ranging from 15 to 25 nm (Figure 5B, vii−ix). Accompanying the formation of the BSA PIC shell was a considerable increase in the capsule yield and ATC encapsulation efficiency, which increased from 54.6% at pH 5.0 to 72.0% at pH 3.0 (Figure S13). In the case of fully polysaccharide capsules, since the pK_a values of chitosan, pectin, and xanthan gum are approximately 6.2, 3.5, and 2.6, respectively, we adjusted the pH (2) of the suspension to a higher value (4.6), thus forming the PIC shell with either pectin (Figure 5D) or xanthan gum (Figure 5E). It is interesting to emphasize that the generation of the polysaccharide PIC shell was triggered by increasing the pH, which is the opposite trend as the polysaccharide-BSA capsules. Such pH-dependent formation could provide more versatility in terms of designing various core−shell−shell nanostructures for the delivery of pH-sensitive bioactives. Another advantage of our strategy is the direct use of the non-cross-linked materials in the as-prepared shell cross-linked capsule suspension, avoiding the multistep addition of shell materials, such as through layer-by-layer polyelectrolyte deposition, which can cause substantial dilution of the bioactive loading.

Delivery Performance. We hypothesized that the generation of the PIC shell would confer the nanocapsules with additional protection and functionality. We used the ratio of pyrene monomer fluorescence emission at 373 and 383 nm (I_1/I_3) to monitor changes in the micropolarity of the environment surrounding the pyrene.[38] The results showed that the fluorescence intensity of pyrene increased with the formation of the PIC shell, and meanwhile the I_1/I_3 values decreased (Figure 6A), indicating a low micropolarity environment inside the nanocapsules.[39] The generation of PIC/cross-linked double shells creates more hydrophobic domains inside the nanocapsules, which could help decrease the exposure of bioactives to the harsh aqueous environment. This conclusion was supported by stability assays of ATC-containing formulations under exposure to ascorbic acid, auto-oxidation, and heat (Figure 6B). Whatever the treatment, the core−shell−shell nanocapsules exhibited only the slightest color fade and degradation of ATC (Figure S14). For example, the degradation of ATC in the presence of ascorbic acid was decreased by 38.2% in the core−shell−shell nanocapsules. Such stabilizing effect was attributed to the high penetration barrier provided by the dense double shells against polar-

DOI: 10.1021/acsnano.9b03049
ACS Nano 2019, 13, 9016−9027

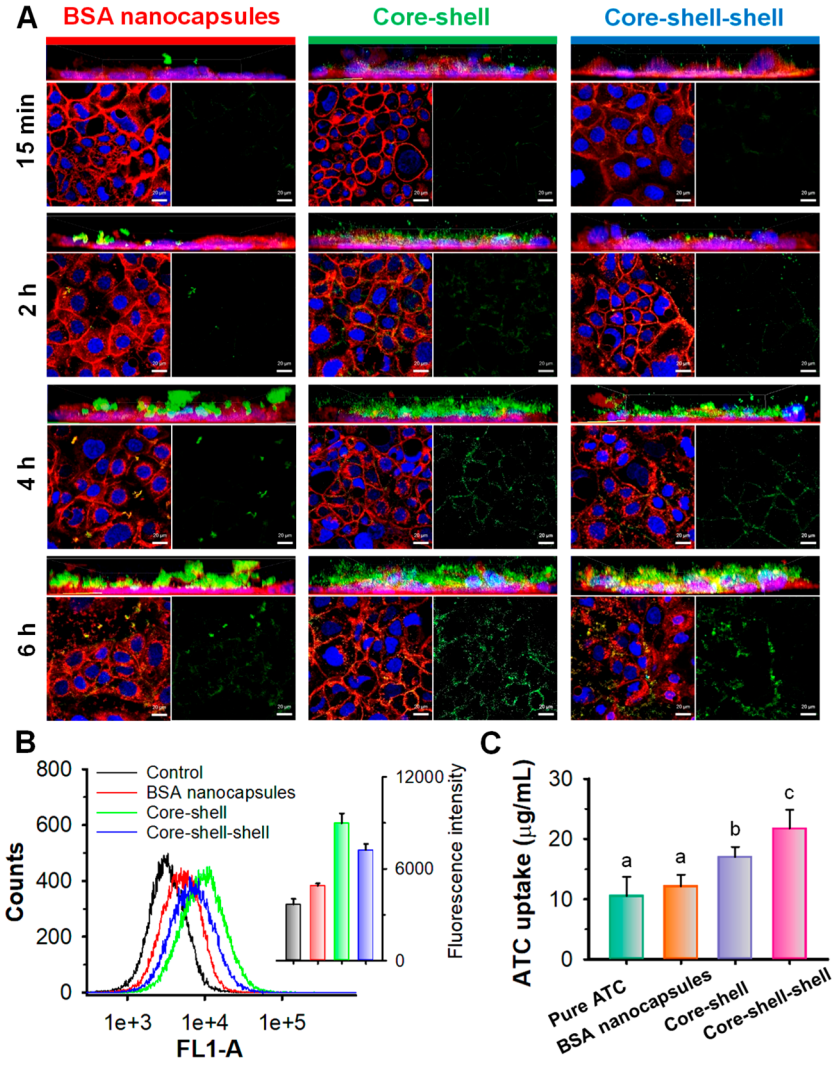

Figure 7. Uptake of the BSA nanocapsules and CHS-BSA nanocapsules (core−shell and core−shell−shell) in Caco-2 cells. (A) Confocal laser scanning imaging of Caco-2 treated with the FITC-labeled nanocapsules for 15 min, 2 h, 4 h, and 6 h. Cell nucleus stained with Hoechst 33342 (blue) and cell membrane stained with CellMask Orange (red); FITC shown in green fluorescence. In each figure group, the upper shows the 3D projections of the Caco-2 monolayer, the bottom left shows the merged signals, while the bottom right shows the FITC signal distributed in the nanocapsules. (B) Flow cytometry of Caco-2 cells after 6 h incubation with the nanocapsules. The red shift of the intensity curves indicates the nanocapsule accumulation in the cells. The inset shows the corresponding median fluorescent intensity. Control is the blank cells. (C) ATC cellular uptake after 6 h incubation with the Caco-2 cells. Different letters represent a significant difference ($P < 0.05$). Data represent mean ± SD, $n = 6$.

oxidants (*e.g.,* oxygen and ascorbic acid) and hydrolysis by water attack.[40] The core−shell−shell nanocapsules also had much higher loading capacity, as the loading content was progressively increased within the studied concentration range (Figure 6C). By contrast, the core−shell nanocapsules were almost saturated by 2.25% of the initially added content of ATC, corresponding to a loading content of 1.06%.

More interestingly, such composite double shells are driven by both covalent bonding and electrostatic complexation, thus the nanocapsules could have responsiveness to diverse stimuli, such as pH and reduction. Figure 6D shows that at pH 1.3 (simulating the pH of the human stomach), only 39% and 34% of encapsulated ATC released from the core−shell and core−shell−shell nanocapsules after 6 h, respectively; such small release could reduce the gastric degradation of the encapsulated bioactive. At pH 6.2 (simulating the pH in the intestine), the nanocapsules also released a small amount of ATC over 12 h. These results can be explained by the high pH tolerance of the cross-linked shell, evidenced by the structural integrity of the nanocapsules from TEM observations (Figure 6D, inset). Note that ATC release was further delayed in the core−shell−shell nanocapsules compared to that in the core−shell nanocapsules. We attributed this to the slow dissociation process of the outer PIC shell, which can still be seen after 4 h incubation (Figure 6D, inset). This slow and sustained release pattern in the intestine can facilitate the bioaccessibility of bioactives.[41]

To confirm the redox-responsive ability, we then treated the nanocapsules in the presence of glutathione (GSH), a biological thiol found within cells.[42] In the case of using 20 μM of GSH at pH 6.2 (simulating the extracellular concentration of GSH), the release behaviors of ATC did not significantly change (Figure 6E). When the GSH concentration was increased to 10 mM (simulating the intracellular concentration of GSH), the release process of ATC clearly accelerated. For the core−shell nanocapsules, a

DOI: 10.1021/acsnano.9b03049
ACS Nano 2019, 13, 9016−9027

burst release was triggered during the initial 2.5 h incubation period and then up to 74% of ATC released after 12 h. Accompanying this observation was the appearance of many small irregular fragments in the TEM imaging, which indicated the serious disassembly of the cross-linked capsule shell by GSH reduction (Figure 6E, inset). Due to its reduction insensitivity, the PIC shell can effectively delay the structural disassembly, thus allowing a sustained release of ATC. Considering these observations, we believe that the core−shell−shell nanocapsule can serve as a controlled delivery system for bioactives in both the gastrointestinal tract and cellular environment.[43]

Finally, we evaluated the cellular internalization of our nanocapsules by the Caco-2 cells, an *in vitro* model simulating drug uptake into human intestine. We chose three formulations including CHS-BSA core−shell nanocapsules (~149.4 nm, PDI 0.20), core−shell−shell nanocapsules (~169.2 nm, PDI 0.24), and the BSA nanocapsules without CHS (~185.7 nm, PDI 0.32) as a control. We first evaluated the cytotoxicity of these nanocapsules in Caco-2 cells and found that after 24 h incubation, over 97% of the cells can survive in the capsule suspension even at a concentration as high as 655 μg/mL (Figure S15), indicating their high biocompatibility. To study the intracellular uptake of nanocapsules, we labeled them by adding fluorescein isothiocyanate (FITC)-BSA and then incubated with Caco-2 monolayer. The confocal laser scanning microscope (CLSM) images show that both the core−shell and core−shell−shell nanocapsules can maintain homogeneous dispersion in the cell medium as evidenced by their dot-like fluorescence, whereas the BSA nanocapsules took the form of large aggregates (Figure S16). The 3D projections demonstrate the accumulation of FITC signal (green fluorescence) in the internal cellular plane over time. Note that most of the BSA nanocapsules were found to collect on the apical surface of the cells after 6 h incubation (Figure 7A) rather than internalize fully, probably due to the large size of the aggregates. The CHS-BSA nanocapsules had a greater extent of internalization. They rapidly attached to the Caco-2 monolayer membrane surface even after 15 min incubation and were significantly internalized into the cytoplasm after 2 h. Flow cytometry data confirmed that after 6 h incubation, the fluorescence intensity of core−shell and core−shell−shell nanocapsules was 1.83- and 1.48-fold higher than that of the BSA nanocapsules (Figure 7B). We attributed this to the good dispersity of CHS-BSA nanocapsules in the cell medium and the presence of CHS that can be easily internalized in Caco-2 cells *via* CD44 receptor-mediated endocytosis.[44,45]

The easy internalization suggests the potential of CHS-BSA nanocapsules as excellent carriers for drug delivery. In our case, the uptake of pure ATC from blueberry extracts was 10.54 μg/mL corresponding to the absorption efficiency of 2.10%, close to the reported values (1−4%) of blueberry ATC in Caco-2 cells.[46] Our CHS-BSA nanocapsules demonstrated a significant improvement ($p < 0.05$) of the ATC amount internalized by Caco-2 cells (Figure 7C). The highest cellular uptake of ATC was observed for the core−shell−shell nanocapsules, 2.06-fold higher than that of pure ATC. It was also noteworthy that although the core−shell nanocapsules had the highest cell internalization, their ATC uptake was moderate compared to the core−shell−shell nanocapsules. This interesting observation could be related to the stability of ATC itself in the cell medium (pH 7.4), as ATC demonstrates serious degradation at neutral pH.[40] Indeed, we found that approximately 65% of pure ATC degraded after 6 h incubation with cells (Figure S17). By contrast, the nanocapsules can effectively protect ATC from degradation in cell medium. This stabilization was the most pronounced for the core−shell−shell nanocapsules, thus enabling more ATC available for adsorption in the intestine.

CONCLUSIONS

We have developed a stable, effective, and multifunctional aqueous core−shell−shell nanostructured platform for the delivery of hydrophilic bioactive agents. The synthesis is simple, general, scalable, and environmentally friendly and does not require multiple emulsification steps, substantial dilution, the use of specialized equipment, organic solvents, or synthetic copolymers as required in conventional methods. In our approach, the formation of the aqueous core nanocapsules with double nanoshells is driven by both covalent bonding and electrostatic interaction through successive cross-linking and interfacial complexation. Such core−shell−shell nanocapsules are highly biocompatible and present attractive features in high encapsulation efficiency, loading content, strong resistance against environmental changes, the ability to respond to external stimuli (*e.g.*, pH- and redox-responsive release), and high cellular uptake. We have also demonstrated that our approach is versatile for introducing multifunctionalities to nanocapsules using various shell materials, with the only requirement being that they can be cross-linked during the acoustic cavitation process. This method can be used to encapsulate a wide array of hydrophilic bioactive molecules, nanocomplexes, and water-dispersible inorganic nanomaterials. We believe that this encapsulation strategy and resulting stimuli-responsive core−shell−shell nanosystem should be of interest for both fundamental research and applications based on the controlled delivery of hydrophilic bioactives and nanomaterials.

EXPERIMENTAL SECTION

Materials. BSA (fraction V, 98% purity) was purchased from CalBiochem (catalog number 12659). Fluorescein-conjugated bovine serum albumin (FITC-BSA was purchased from Life Technologies (catalog number A23015, Invitrogen, Life Technologies). HCS CellMask Orange Stain, Hoechst 33342, and DMEM/F-12 were purchased from Thermo Fisher Scientific. CHS-type A from bovine trachea cartilage (M_w = 5−10 kDa) was purchased from Bulk Supplements (Henderson, NV, US). EG (99% purity) was purchased from ACROS Organics. Pectin powder from citrus peel, chitosan of medium molecular weight (M_w = 190−310 kDa, 75−85% degree of deacetylation, viscosity 200−800 cP), dextran sulfate, sodium dodecyl sulfate (SDS), Span 80, GSH, L-ascorbic acid (99% purity), folic acid (≥97% purity), and methyl blue were purchased from Sigma-Aldrich (St. Louis, MO, US). Calcium-D-pantothenate was donated by BASF. The κ-carrageenan was acquired by TIC Gums, Incorporated (White Marsh, MD). Xanthan gum was purchased from Colony Gums (Monroe, NC). 100% pure corn oil (Mazola, ACH Food Companies, Inc., Cordova, TN) was purchased from a local supermarket. The ATC source was a blueberry extract obtained from Bulk Supplements; the ATC content in this extract was calculated to be approximately 25% (w/w) according to the protocol outlined using the pH differential method.[14] Dry beet root powder was obtained from Bulk Supplements (Henderson, NV) for use as the betanin source. Liquid "Spirulina Blue" phycocyanin was extracted from DDW The Color House (Louisville, KY), in which the phycocyanin content of this source was estimated to be 43 ± 5 mg/g liquid extract. Methyl orange was purchased from Matheson Coleman and Bell (Norwood, Ohio).

DOI: 10.1021/acsnano.9b03049
ACS Nano 2019, 13, 9016−9027

Rhodamine 6G was purchased from Allied Chemical Corporation (New York). The inorganic nanomaterials including halloysite nanotube, Fe_3O_4 nanoparticle, CuO nanoparticle, TiO_2 nanoparticle, and TiO_2 nanotube were synthesized using our previous methods (see Supporting Information for more details). All other reagents used were of analytical grade.

Fabrication of Core−Shell Nanocapsules. Core−shell nanocapsules were synthesized *via* an inverse mini-emulsion polymerization method as described by Suslick[23] and Bradely *et al.*,[47] with some modifications. A schematic of the procedure is illustrated in Figure 1A. Taking the core−shell nanostructure with the incorporation of ATC as an example, the aqueous phase consisted of 4 mL of CHS (0.5%, w/w), 4 mL of BSA solution (0.5%, w/w), and 0.7 mL ATC solution. To prevent complex formation after mixing, the pH values of the individual CHS, BSA, and ATC solutions were adjusted to 5 using hydrochloric acid before mixing. When evaluating the ATC loading content, the initial concentration ($m_{ATC}/m_{(BSA+polysaccharide)}$, % w/w) of ATC was set at 0.75%, 1.25%, 1.75%, 2.25%, 2.88%, and 3.5%. A total of 20 mL of corn oil with 0.3 g of Span 80 was used as the oil phase, which was layered on the above aqueous phase in a glass vial. The water-in-oil inverse mini-emulsion template was prepared by high-intensity ultrasound using a 750 W ultrasonic processor with a high-power sonic tip operated at 20 kHz frequency (VC 750, Sonics vibra-cell, Sonics & Materials, Newtown, CT, USA). The bottom of the 13 mm diameter ultrasonic probe was immersed at the oil−water interface, and the system was sonicated for 8 min at an acoustic intensity of 300 W cm^{-2} (5 s on, 2 s off). During the sonication, the system was kept in an ice bath, allowing to increase the chemical yield of radicals at low temperature.[48,49] The obtained fine emulsion was then transferred into a centrifuge tube and centrifuged at 2000 *g* for 5 min to remove the oil phase and fragments. The residual oil was further removed by twice washing with deionized water (pH 5) using a centrifugation (15,000 *g*, 10 min)/washing protocol.[14] The oil-free samples, that is, aqueous core−shell nanocapsules, were transferred into vials and stored in a refrigerator until use (4 °C in the dark), which was labeled as ATC-CHS-BSA. To prepare the nanocomplex-incorporated nanocapsules (ATC-EG-CHS-BSA), the ATC-EG-CHS co-pigmentation nanocomplexes were first prepared at pH 5 (experimental procedures are provided in the Supporting Information), followed by mixing with BSA solution. The ultrasound condition was the same as described above. For comparison, ATC-loaded BSA nanocapsules (ATC-BSA) without the addition of CHS and EG were prepared as a control in the same way.

Other types of polysaccharide-protein nanocapsules were prepared using combinations of κ-carrageenan-BSA, dextran sulfate-BSA, pectin-BSA, and xanthan gum-BSA. The pH of each solution (0.5%, w/w) in these combinations was adjusted to 5. Similarly, these polysaccharides were combined with BSA solution and the oil phase for further ultrasound treatment. For the preparation of fully polysaccharide-based capsules, the combinations of pectin-chitosan and xanthan gum-chitosan were used. The pH of each polysaccharide solution (0.5%, w/w) was adjusted to 2 before mixing in order to avoid any complexation. Afterward, the two polysaccharide solutions were mixed at a ratio of 1:1 and added to 20 mL of the oil phase (corn oil + Span 80) for further ultrasound treatment.

To verify the universality of these nanocapsules, various kinds of hydrophilic compounds (betanin, norbixin, chlorophyll, phycocyanin, methyl blue, methyl orange, rhodamine 6G, ascorbic acid, calcium pantothenate, and folic acid) and water-dispersible inorganic nanomaterials (halloysite nanotubes, CuO nanoparticles, Fe_3O_4 nanoparticles, TiO_2 nanoparticles, and TiO_2 nanotubes) were used instead of ATC for the CHS-BSA nanocapsule loads.

Fabrication of Core−Shell−Shell Nanocapsules. Core−shell−shell nanocapsules were prepared by depositing excess non-cross-linked materials on the surface of shell cross-linked nanocapsules. After obtaining the core−shell nanocapsules with the incorporation of nanocomplexes, the pH (5) of the nanocapsule suspension was carefully adjusted to lower values (2.5−4.5) using 10% (v/v) hydrochloric acid. During this process, the non-cross-linked protein molecules became positively charged and deposited on the negatively charged nanocapsules by electrostatic attraction, creating an additional PIC shell. The final samples were transferred into vials and stored in a refrigerator until use (4 °C in the dark). In the case of fully polysaccharide-based capsules, the pH was switched from 2 to 4.6 to trigger the generation of the polysaccharide PIC shell.

Characterizations. SEM was performed on a LEO 1550 SEM equipped with a GEMINI field emission column. Cryo-focused ion beam (cryo-FIB) was used to characterize the core−shell−shell nanostructure. Briefly, aliquots of 1 mL of fresh aqueous capsule suspension was diluted to 10 mL with the phosphate buffer of the same pH, which was then snap-frozen by immediately plunging it into slush nitrogen and transferred under vacuum into a FEI Strata 400 FIB fitted with a Quorum PP3010T Cryo-FIB/SEM Preparation System (Quorum Technologies, Newhaven, U.K.). The sample was then maintained at −165 °C for the duration of the experiment and coated with gold−palladium. To get a cross section of interface, a focused gallium ion beam was applied to mill through the nanostructure. For TEM observation, the samples were also diluted by 10 times with phosphate buffer, and the images were taken using a FEI T12 Spirit TEM STEM operated at 120 kV.[50] The thickness of the shell was calculated from 50 individual capsules in the TEM images using ImageJ software. CLSM imaging was performed on a Zeiss LSM 700 confocal microscope (Zeiss, Oberkochen, Germany). XPS was performed to study the chemical state of the shell materials using a Surface Science Instruments SSX-100 XPS system at an operating pressure of ~2×10^{-9} Torr. Thermogravimetric curves were obtained from a thermogravimetric analyzer (TGA Q500, TA Instruments, New Castle, DE, USA) (see the Supporting Information). Average diameter and ζ potential were determined by the dynamic light scattering technique (see the Supporting Information). The capsule yield was calculated by weighing the residual capsule pellet after centrifugation (15000 *g* for 10 min) (see the Supporting Information). The encapsulation efficiency of ATC and other hydrophilic compounds in the nanocapsules was determined from the supernatant after centrifuging the samples (see the Supporting Information). Electrophoresis of protein was evaluated by sodium dodecyl sulfate-polyacrylamide gel electrophoresis (SDS-PAGE) (see the Supporting Information). The micropolarity inside the capsules was evaluated from the pyrene fluorescence (see the Supporting Information). The *in vitro* pH- and GSH-responsive release of ATC was determined based on the membrane free-model (see the Supporting Information). Cellular assays (cell cultural, cell viability, endocytosis, CLSM internalization assay, ATC cellular uptake, and degradation) were evaluated using human colon adenocarcinoma cells and Caco-2 cells (see the Supporting Information).

ASSOCIATED CONTENT

Supporting Information

The Supporting Information is available free of charge on the ACS Publications website at DOI: 10.1021/acsnano.9b03049.

Synthesis of co-pigmentation complexes; additional characterization and performance of nanocapsules including capsule yield, encapsulation efficiency, stability assays, *in vitro* release, thermogravimetric analysis, particle size and ζ potential, ATR-FTIR spectra, electrophoresis, and UV−vis spectra; synthesis of inorganic nanoparticles; photocatalytic experiment; cellular assays including Caco-2 cell culture, cell viability, endocytosis, CLSM internalization, cellular uptake, and degradation (PDF)

AUTHOR INFORMATION

Corresponding Author

*E-mail: alireza@cornell.edu.

DOI: 10.1021/acsnano.9b03049
ACS Nano 2019, 13, 9016−9027

ORCID

Mohammad Arshadi: 0000-0003-2387-4803
Michelle C. Lee: 0000-0002-2584-7772
Alireza Abbaspourrad: 0000-0001-5617-9220

Notes

The authors declare no competing financial interest.

ACKNOWLEDGMENTS

We thank the Cornell Center for Materials Research (CCMR) for use of their facilities. CCMR facilities are supported by the National Science Foundation under award number DMR-1719875. We would also like to acknowledge the BASF Corporation for their continued support of academic and research pursuits.

REFERENCES

(1) Anselmo, A. C.; McHugh, K. J.; Webster, J.; Langer, R.; Jaklenec, A. Layer-by-Layer Encapsulation of Probiotics for Delivery to the Microbiome. *Adv. Mater.* **2016**, *28*, 9486−9490.
(2) Li, Z.; Behrens, A. M.; Ginat, N.; Tzeng, S. Y.; Lu, X.; Sivan, S.; Langer, R.; Jaklenec, A. Biofilm-Inspired Encapsulation of Probiotics for the Treatment of Complex Infections. *Adv. Mater.* **2018**, *30*, 1803925.
(3) Wang, Y.; Shim, M. S.; Levinson, N. S.; Sung, H. W.; Xia, Y. Stimuli-Responsive Materials for Controlled Release of Theranostic Agents. *Adv. Funct. Mater.* **2014**, *24*, 4206−4220.
(4) Karimi, M.; Sahandi Zangabad, P.; Baghaee-Ravari, S.; Ghazadeh, M.; Mirshekari, H.; Hamblin, M. R. Smart Nanostructures for Cargo Delivery: Uncaging and Activating by Light. *J. Am. Chem. Soc.* **2017**, *139*, 4584−4610.
(5) Kim, S. H.; Kim, K. R.; Ahn, D. R.; Lee, J. E.; Yang, E. G.; Kim, S. Y. Reversible Regulation of Enzyme Activity by PH-Responsive Encapsulation in DNA Nanocages. *ACS Nano* **2017**, *11*, 9352−9359.
(6) McClements, D.; Encapsulation, J. Protection, and Release of Hydrophilic Active Components: Potential and Limitations of Colloidal Delivery Systems. *Adv. Colloid Interface Sci.* **2015**, *219*, 27−53.
(7) Aditya, N. P.; Espinosa, Y. G.; Norton, I. T. Encapsulation Systems for the Delivery of Hydrophilic Nutraceuticals: Food Application. *Biotechnol. Adv.* **2017**, *35*, 450−457.
(8) Dickinson, E. Colloids in Food: Ingredients, Structure, and Stability. *Annu. Rev. Food Sci. Technol.* **2015**, *6*, 211−233.
(9) Mehnert, W.; Mäder, K. Solid Lipid Nanoparticles: Production, Characterization and Applications. *Adv. Drug Delivery Rev.* **2012**, *64*, 83−101.
(10) Devi, N.; Sarmah, M.; Khatun, B.; Maji, T. K. Encapsulation of Active Ingredients in Polysaccharide−Protein Complex Coacervates. *Adv. Colloid Interface Sci.* **2017**, *239*, 136−145.
(11) Luo, R.; Venkatraman, S. S.; Neu, B. Layer-by-Layer Polyelectrolyte-Polyester Hybrid Microcapsules for Encapsulation and Delivery of Hydrophobic Drugs. *Biomacromolecules* **2013**, *14*, 2262−2271.
(12) Xuan, M.; Zhao, J.; Shao, J.; Du, C.; Cui, W.; Duan, L.; Qi, W.; Li, J. Recent Progresses in Layer-by-Layer Assembled Biogenic Capsules and Their Applications. *J. Colloid Interface Sci.* **2017**, *487*, 107−117.
(13) Ishii, S.; Kaneko, J.; Nagasaki, Y. Development of a Long-Acting, Protein-Loaded, Redox-Active, Injectable Gel Formed by a Polyion Complex for Local Protein Therapeutics. *Biomaterials* **2016**, *84*, 210−218.
(14) Tan, C.; Celli, B. G.; Lee, M.; Licker, J.; Abbaspourrad, A. Polyelectrolyte Complex Inclusive Biohybrid Microgels for Tailoring Delivery of Copigmented Anthocyanins. *Biomacromolecules* **2018**, *19*, 1517−1527.
(15) Landfester, K. Miniemulsion Polymerization and the Structure of Polymer and Hybrid Nanoparticles. *Angew. Chem., Int. Ed.* **2009**, *48*, 4488−4507.
(16) Zhao, Y.; Liu, J.; Chen, Z.; Zhu, X.; Möller, M. Hybrid Nanostructured Particles *via* Surfactant-Free Double Miniemulsion Polymerization. *Nat. Commun.* **2018**, *9*, 1918.
(17) Dardelle, G.; Jacquemond, M.; Erni, P. Delivery Systems for Low Molecular Weight Payloads: Core/Shell Capsules with Composite Coacervate/Polyurea Membranes. *Adv. Mater.* **2017**, *29*, 1606099.
(18) Nie, Z.; Xu, S.; Seo, M.; Lewis, P. C.; Kumacheva, E. Polymer Particles with Various Shapes and Morphologies Produced in Continuous Microfluidic Reactors. *J. Am. Chem. Soc.* **2005**, *127*, 8058−8063.
(19) Parker, R. M.; Zhang, J.; Zheng, Y.; Coulston, R. J.; Smith, C. A.; Salmon, A. R.; Yu, Z.; Scherman, O. A.; Abell, C. Electrostatically Directed Self-Assembly of Ultrathin Supramolecular Polymer Microcapsules. *Adv. Funct. Mater.* **2015**, *25*, 4091−4100.
(20) Choi, C. H.; Weitz, D. A.; Lee, C. S. One Step Formation of Controllable Complex Emulsions: From Functional Particles to Simultaneous Encapsulation of Hydrophilic and Hydrophobic Agents into Desired Position. *Adv. Mater.* **2013**, *25*, 2536−2541.
(21) Hasani-Sadrabadi, M. M.; Karimkhani, V.; Majedi, F. S.; Van Dersarl, J. J.; Dashtimoghadam, E.; Afshar-Taromi, F.; Mirzadeh, H.; Bertsch, A.; Jacob, K. I.; Renaud, P.; Stadler, F. J.; Kim, I. L. Microfluidic-Assisted Self-Assembly of Complex Dendritic Polyethylene Drug Delivery Nanocapsules. *Adv. Mater.* **2014**, *26*, 3118−3123.
(22) Kim, M.; Yeo, S. J.; Highley, C. B.; Burdick, J. A.; Yoo, P. J.; Doh, J.; Lee, D. One-Step Generation of Multifunctional Polyelectrolyte Microcapsules *via* Nanoscale Interfacial Complexation in Emulsion (NICE). *ACS Nano* **2015**, *9*, 8269−8278.
(23) Suslick, K. S.; Grinstaff, M. W. Protein Microencapsulation of Nonaqueous Liquids. *J. Am. Chem. Soc.* **1990**, *112*, 7807−7809.
(24) Han, Y.; Shchukin, D.; Yang, J.; Simon, C. R.; Fuchs, H.; Möhwald, H. Biocompatible Protein Nanocontainers for Controlled Drugs Release. *ACS Nano* **2010**, *4*, 2838−2844.
(25) Tzhayik, O.; Cavaco-Paulo, A.; Gedanken, A. Fragrance Release Profile from Sonochemically Prepared Protein Microsphere Containers. *Ultrason. Sonochem.* **2012**, *19*, 858−863.
(26) Cavalieri, F.; Ashokkumar, M.; Grieser, F.; Caruso, F. Ultrasonic Synthesis of Stable, Functional Lysozyme Microbubbles. *Langmuir* **2008**, *24*, 10078−10083.
(27) Grinstaff, M. W.; Suslick, K. S. Air-Filled Proteinaceous Microbubbles: Synthesis of an Echo-Contrast Agent. *Proc. Natl. Acad. Sci. U. S. A.* **1991**, *88*, 7708−7710.
(28) Tan, C.; Lee, M. C.; Pajoumshariati, S.; Abbaspourrad, A. Sonochemically Synthesized Ultrastable High Internal Phase Emulsions *via* a Permanent Interfacial Layer. *ACS Sustainable Chem. Eng.* **2018**, *6*, 14374−14382.
(29) Cortez, R.; Luna-Vital, D. A.; Margulis, D.; Gonzalez de Mejia, E. Natural Pigments: Stabilization Methods of Anthocyanins for Food Applications. *Compr. Rev. Food Sci. Food Saf.* **2017**, *16*, 180−198.
(30) Jeong, D.; Bae, B. C.; Park, S. J.; Na, K. Reactive Oxygen Species Responsive Drug Releasing Nanoparticle Based on Chondroitin Sulfate-Anthocyanin Nanocomplex for Efficient Tumor Therapy. *J. Controlled Release* **2016**, *222*, 78−85.
(31) Arshadi, M.; Eskandarloo, H.; Enayati, M.; Godec, M.; Abbaspourrad, A. Highly Water-Dispersible and Antibacterial Magnetic Clay Nanotubes Functionalized with Polyelectrolyte Brushes: High Adsorption Capacity and Selectivity Toward Heparin in Batch and Continuous System. *Green Chem.* **2018**, *20*, 5491−5508.
(32) Tawil, N.; Sacher, E.; Boulais, E.; Mandeville, R.; Meunier, M. X-Ray Photoelectron Spectroscopic and Transmission Electron Microscopic Characterizations of Bacteriophage-Nanoparticle Complexes for Pathogen Detection. *J. Phys. Chem. C* **2013**, *117*, 20656−20665.
(33) Borodina, T. N.; Grigoriev, D. O.; Carillo, M. A.; Hartmann, J.; Moehwald, H.; Shchukin, D. G. Preparation of Multifunctional Polysaccharide Microcontainers for Lipophilic Bioactive Agents. *ACS Appl. Mater. Interfaces* **2014**, *6*, 6570−6578.

DOI: 10.1021/acsnano.9b03049
ACS Nano 2019, 13, 9016−9027

(34) Tan, C.; Pajoumshariati, S.; Arshadi, M.; Abbaspourrad, A. A Simple Route to Renewable High Internal Phase Emulsions (HIPEs) Strengthened by Successive Cross-Linking and Electrostatics of Polysaccharides. *Chem. Commun.* **2019**, *55*, 1225−1228.
(35) Guerrini, L.; Alvarez-Puebla, R.; Pazos-Perez, N. Surface Modifications of Nanoparticles for Stability in Biological Fluids. *Materials* **2018**, *11*, 1154.
(36) Mu, Q.; Jiang, G.; Chen, L.; Zhou, H.; Fourches, D.; Tropsha, A.; Yan, B. Chemical Basis of Interactions between Engineered Nanoparticles and Biological Systems. *Chem. Rev.* **2014**, *114*, 7740−7781.
(37) Feld, A.; Koll, R.; Fruhner, L. S.; Krutyeva, M.; Pyckhout-Hintzen, W.; Weiß, C.; Heller, H.; Weimer, A.; Schmidtke, C.; Appavou, M. S.; Kentzinger, E.; Allgaier, J.; Weller, H. Nanocomposites of Highly Monodisperse Encapsulated Superparamagnetic Iron Oxide Nanocrystals Homogeneously Dispersed in a Poly(Ethylene Oxide) Melt. *ACS Nano* **2017**, *11*, 3767−3775.
(38) Kalyanasundaram, K.; Thomas, J. K. Environmental Effects on Vibronic Band Intensities in Pyrene Monomer Fluorescence and Their Application in Studies of Micellar Systems. *J. Am. Chem. Soc.* **1977**, *99*, 2039−2044.
(39) Tan, C.; Celli, G. B.; Abbaspourrad, A. Copigment-Polyelectrolyte Complexes (PECs) Composite Systems for Anthocyanin Stabilization. *Food Hydrocolloids* **2018**, *81*, 371−379.
(40) Trouillas, P.; Sancho-García, J. C.; De Freitas, V.; Gierschner, J.; Otyepka, M.; Dangles, O. Stabilizing and Modulating Color by Copigmentation: Insights from Theory and Experiment. *Chem. Rev.* **2016**, *116*, 4937−4982.
(41) McClements, D. J. The Future of Food Colloids: Next-Generation Nanoparticle Delivery Systems. *Curr. Opin. Colloid Interface Sci.* **2017**, *28*, 7−14.
(42) Carelli, S.; Ceriotti, A.; Cabibbo, A.; Fassina, G.; Ruvo, M.; Sitia, R. Cysteine and Glutathione Secretion in Response to Protein Disulfide Bond Formation in the ER. *Science (Washington, DC, U. S.)* **1997**, *277*, 1681−1684.
(43) Shu, S.; Zhang, X.; Wu, Z.; Wang, Z.; Li, C. Gradient Cross-Linked Biodegradable Polyelectrolyte Nanocapsules for Intracellular Protein Drug Delivery. *Biomaterials* **2010**, *31*, 6039−6049.
(44) Lo, Y.-L.; Sung, K.-H.; Chiu, C.-C.; Wang, L.-F. Chemically Conjugating Polyethylenimine with Chondroitin Sulfate to Promote CD44-Mediated Endocytosis for Gene Delivery. *Mol. Pharmaceutics* **2013**, *10*, 664−676.
(45) Cho, H.-J.; Oh, J.; Choo, M.-K.; Ha, J.-I.; Park, Y.; Maeng, H.-J. Chondroitin Sulfate-Capped Gold Nanoparticles for the Oral Delivery of Insulin. *Int. J. Biol. Macromol.* **2014**, *63*, 15−20.
(46) Kamiloglu, S.; Capanoglu, E.; Grootaert, C.; Van Camp, J. Anthocyanin Absorption and Metabolism by Human Intestinal Caco-2 Cells—A Review. *Int. J. Mol. Sci.* **2015**, *16*, 21555−21574.
(47) Bradley, M.; Ashokkumar, M.; Grieser, F. Sonochemical Production of Fluorescent and Phosphorescent Latex Particles. *J. Am. Chem. Soc.* **2003**, *125*, 525−529.
(48) Bradley, M. A.; Prescott, S. W.; Schoonbrood, H. A. S.; Landfester, K.; Grieser, F. Miniemulsion Copolymerization of Methyl Methacrylate and Butyl Acrylate by Ultrasonic Initiation. *Macromolecules* **2005**, *38*, 6346−6351.
(49) Cooper, G.; Grieser, F.; Biggs, S. Butyl Acrylate/Vinyl Acetate Copolymer Latex Synthesis Using Ultrasound as an Initiator. *J. Colloid Interface Sci.* **1996**, *184*, 52−63.
(50) Lee, M. C.; Tan, C.; Abbaspourrad, A. Combination of Internal Structuring and External Coating in an Oleogel-Based Delivery System for Fish Oil Stabilization. *Food Chem.* **2019**, *277*, 213−221.

DOI: 10.1021/acsnano.9b03049
ACS Nano 2019, 13, 9016−9027